THE JOURNAL OF PHYSICAL CHEMISTRY C
A JOURNAL OF THE AMERICAN CHEMICAL SOCIETY

pubs.acs.org/JPCC

Article

Improving the Cycle Life of Solid-State Batteries by Addition of Oxide Nanoparticles to a Complex Hydride Solid Electrolyte

Laura de Kort, Peter Ngene, Marcello Baricco, Petra de Jongh,* and Valerio Gulino*

Cite This: *J. Phys. Chem. C* 2023, 127, 3988−3995

Read Online

ACCESS | Metrics & More | Article Recommendations | Supporting Information

ABSTRACT: We report that the addition of silica nanoparticles to the iodide-substituted $LiBH_4$ (h-$Li(BH_4)_{0.8}(I)_{0.2}$) improves the ion conductivity and, remarkably, the cycle life of the all-solid state batteries. The h-$Li(BH_4)_{0.8}(I)_{0.2}$-SiO_2 was synthesized by mechanochemical treatment and possesses a Li^+ conductivity of 9.3×10^{-5} S cm^{-1} at RT. It has an electrochemical stability window of about 2.5 V vs Li^+/Li and an improved stability against Li-metal, compared to h-$Li(BH_4)_{0.8}(I)_{0.2}$, owing to the addition of oxide nanoparticles, which we ascribed to a greater mechanical stability of the solid-state electrolyte. The all-solid state battery Li|h-$Li(BH_4)_{0.8}(I)_{0.2}$-SiO_2|TiS_2 demonstrated a good long-term cyclability, i.e., over 200 cycles at C/20 and even including a C-rate of C/5, demonstrating that the addition of oxide nanoparticles improves the cycling stability of the electrolyte.

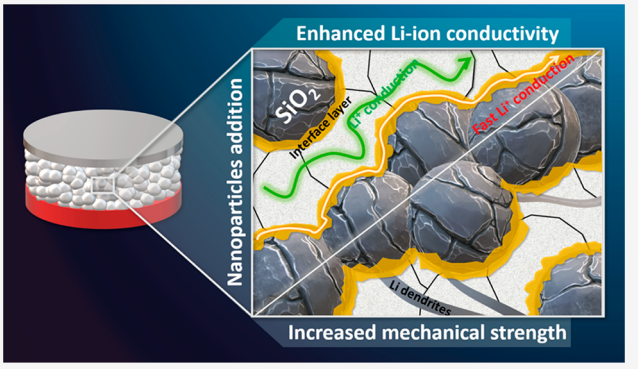

1. INTRODUCTION

Much research effort is devoted to improving the safety of Li-ion batteries, by introducing electrolytes that are thermally stable and not prone to decomposition, thereby limiting the flammability.[1] Solid-state electrolytes are intrinsically less flammable than organic liquid electrolytes. Complex hydrides have shown interesting properties as solid electrolyte, such as a low gravimetric density, a good electrochemical stability and compatibility with Li metal anode (forming stable interface).[2−5] Lithium borohydride ($LiBH_4$), a low density (0.666 g/cm^3) material, has been extensively studied as an electrolyte. Its room temperature (RT) polymorph has an orthorhombic unit cell (o-$LiBH_4$), space group (s.g.) *Pnma*, and low ionic conductivity (σ; around 10^{-8} S cm^{-1}), while the high temperature polymorph, stable above 110 °C, has a hexagonal unit cell (h-$LiBH_4$), s.g. $P6_3mc$,[6] and shows high σ ($\sim 10^{-3}$ S cm^{-1} at 120 °C).[7]

The RT Li-ion conductivity in $LiBH_4$ can be enhanced using different approaches: (a) Halide substitution, replacing BH_4^- with I^-, Br^-, and Cl^-, stabilizes h-$LiBH_4$ forming solid solutions (among them the most conductive composition is h-$Li(BH_4)_{0.8}(I)_{0.2}$);[8−11] (b) Partially decompose the o-$LiBH_4$,[12] also by mixing it with $LiBF_4$;[13] (c) Addition of nanosized oxides to form composites,[3] synthesized by nanoconfinement in suitable scaffolds[14] or by mechanochemical treatment.[15] In the latter, the enhanced Li-ion conductivity relies on the formation of a highly conductive interface layer with the oxide and can be described by a core−shell model.[14,16−18] Even though the $LiBH_4$−oxide interaction is not really understood, it is known that Li-conductivity is optimized when $LiBH_4$ completely fills the oxide pores (adding a $LiBH_4$ volume that corresponds to the oxide total pore volume),[15,19] and the thickness of the interfacial layer has been estimated to be about 2 nm.[20] Recently, the two approaches have been combined, nanoconfining h-$Li(BH_4)_{1-x}(I)_x$ solid solutions in different scaffolds.[21,22]

Studies on $LiBH_4$−oxide composites have mostly focused on improving the conductivity, while little effort has been spent on other important properties, such as mechanical properties, battery assembly, cycle life, and overall battery performance. Here, the synthesis of h-$Li(BH_4)_{0.8}(I)_{0.2}$-SiO_2, with a volume of the h-$Li(BH_4)_{0.8}(I)_{0.2}$ corresponding to that of the pore volume of the oxide nanopowder (i.e., 100% of the oxide pore filled), by mechanochemical treatment, its characterization and its implementation in an all-solid-state battery (SSB) is discussed. We further demonstrate that this material is compatible with a lithium metal anode, and that the addition of SiO_2 enhanced the Li-ion conductivity of the solid electrolyte and greatly enhanced the cyclability, demonstrated with a battery cell using a TiS_2 cathode and Li anode.

Received: December 20, 2022
Revised: February 8, 2023
Published: February 16, 2023

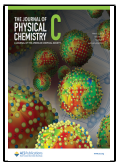

Downloaded via UTRECHT UNIV on December 15, 2023 at 09:30:08 (UTC).
See https://pubs.acs.org/sharingguidelines for options on how to legitimately share published articles.

ACS Publications

© 2023 The Authors. Published by American Chemical Society

https://doi.org/10.1021/acs.jpcc.2c08902
J. Phys. Chem. C 2023, 127, 3988−3995

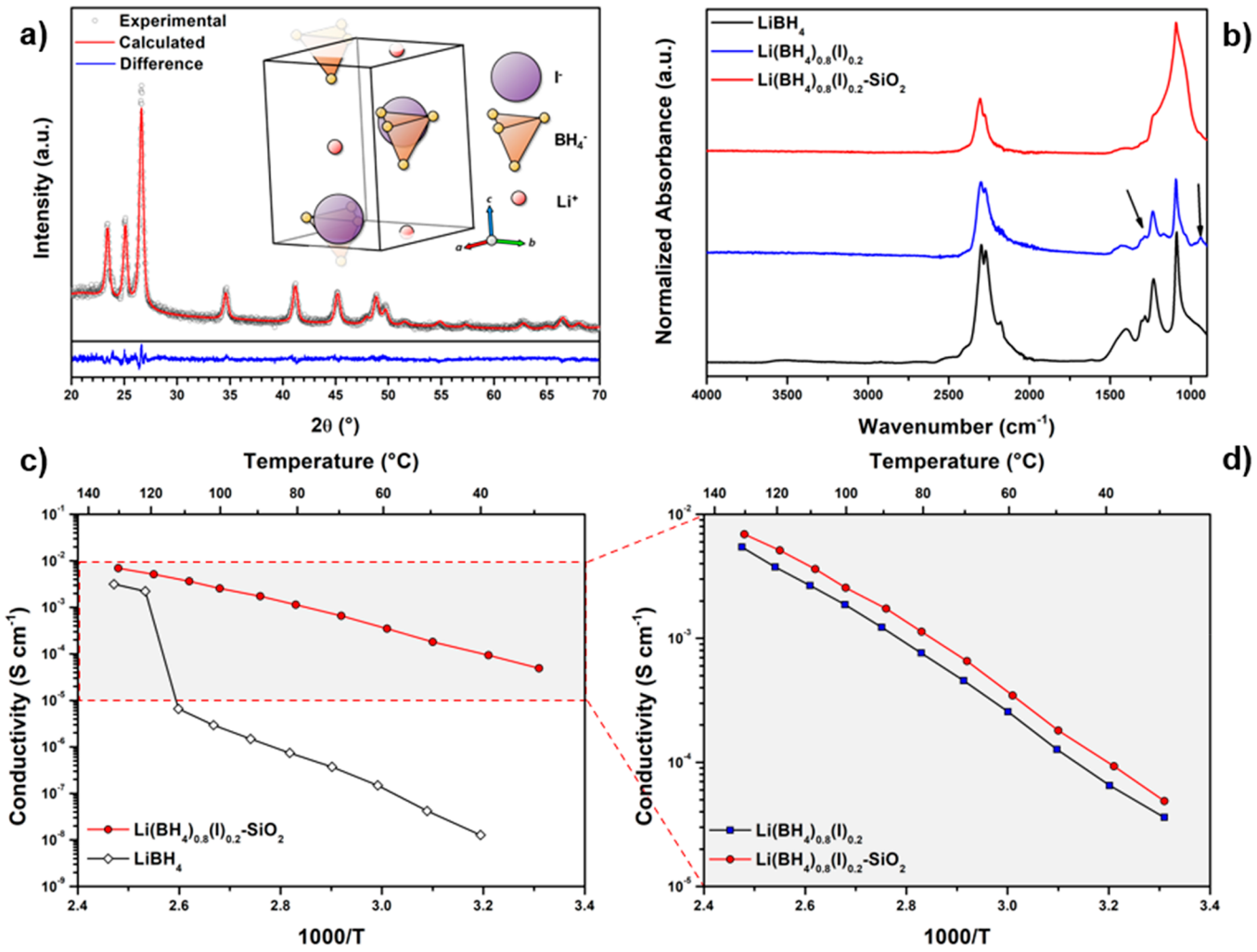

Figure 1. (a) Rietveld refinement of the *h*-$Li(BH_4)_{0.8}(I)_{0.2}$-SiO_2 (SSE) pattern (Rwp 7.03%). The inset shows the structure of the SSE obtained after Rietveld refinement (the relative occupancy of the anions is not shown). (b) ATR spectra of the SSE, *h*-$Li(BH_4)_{0.8}(I)_{0.2}$, and pure $LiBH_4$. Arrows indicate the absorption bands at about 1170 and 960 cm^{-1}. (c) Conductivity of the SSE and pure $LiBH_4$ and (d) of the SSE and *h*-$Li(BH_4)_{0.8}(I)_{0.2}$ obtained during the second heating temperature-dependent EIS cycles.

2. EXPERIMENTAL METHODS

The *h*-$Li(BH_4)_{0.8}(I)_{0.2}$-SiO_2 electrolyte was synthesized according to the procedure and with the composition reported in the Supporting Information (Table S1), and we will refer to it as solid-state electrolyte (SSE). The *h*-$Li(BH_4)_{0.8}(I)_{0.2}$ hexagonal solid solution was stabilized at RT by a combination of mechanochemical treatment and annealing, mixing $LiBH_4$ (purity > 95% from Sigma-Aldrich) and LiI (purity > 99% from Sigma-Aldrich).[11] The SiO_2 nanoparticles (Aerosil 300, Evonik) was incorporated to form a nanocomposite electrolyte by mechanochemical treatment,[15] using a volume of *h*-$Li(BH_4)_{0.8}(I)_{0.2}$ equal to the pore volume of the SiO_2 (i.e., space between the nanoparticles), obtained by N_2 physisorption. The composite was characterized by powder X-ray diffraction (XRD) at RT using a Panalytical X-pert Pro MPD (Cu $K_{\alpha1}$ = 1.54059 Å, $K_{\alpha2}$ = 1.54446 Å) in Debye-Scherer geometry, N_2 adsorption at 77 K in a TriStar Plus II gas-volumetric apparatus (Micromeritics, Norcross, GA, U.S.A.), and by infrared spectroscopy in Attenuated Total Reflection (ATR) with a Bruker Alpha-P spectrometer, equipped with a diamond crystal (see Supporting Information for experimental details).

The conductivity was measured using electrochemical impedance spectroscopy (EIS) on samples obtained by compacting the powder into pellets (diameter 13 mm, thickness 1−2 mm, 150 MPa) using an axial hydraulic press. The total conductivity measured was assigned totally to Li-ion conduction.[4,15] For other electrochemical characterizations, the pellets were obtained by placing about 60 mg of sample powder in PEEK (polyether ether ketone) cylinder (10 mm diameter) and by cold pressing (250 MPa) in between two stainless steel pistons. To measure cyclic voltammetry (CV), the samples were mixed with carbon black (Ketjenblack EC600JD, Akzo Nobel Chemicals) in a weight ratio of 95:5 using an agate mortar.[23] A pellet was obtained by pressing 8 mg of C-SSE mixture on a prepelletized 60 mg of SSE, which was subsequently attached to a Li disk as the counter and reference electrode. For battery-cell assembly, the SSE and TiS_2 (99.9%, Sigma-Aldrich) powders were mixed in a 60:40 weight ratio in an agate pestle for 5 min, and the mixture was used as the composite positive electrode (cathode). A total of 8.9 mg of cathode mixture (3.5 mg of TiS_2) was pressed on top of a pellet prepared using 60 mg of SSE. A freshly polished Li disk as the anode material was pressed with the pellet. These batteries were left for 2 h at 60 °C and then cycled using a

https://doi.org/10.1021/acs.jpcc.2c08902
J. Phys. Chem. C 2023, 127, 3988−3995

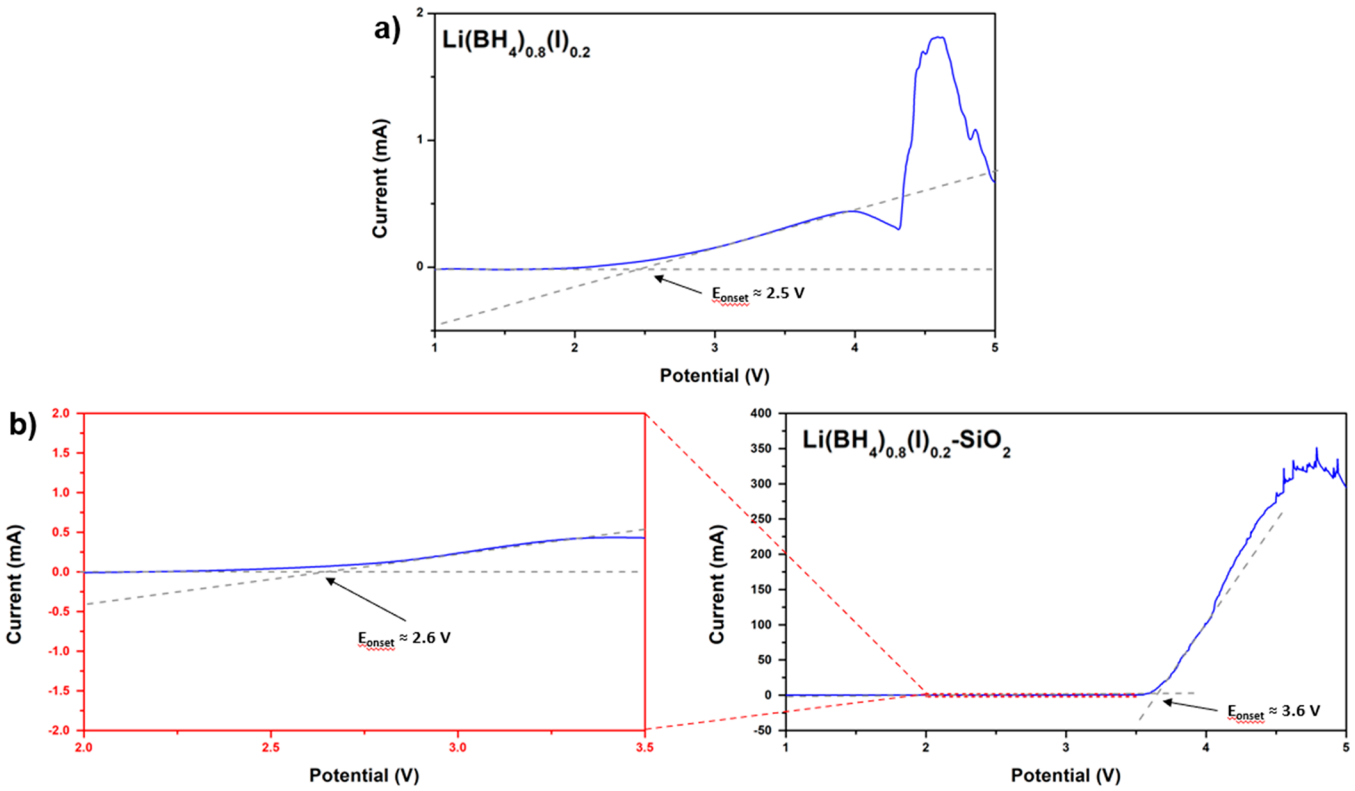

Figure 2. Cyclic voltammetry of Li|*h*-$Li(BH_4)_{0.8}(I)_{0.2}$|*h*-$Li(BH_4)_{0.8}(I)_{0.2}$-C|stainless steel (a) and Li|SSE|SSE-C|stainless steel (b) cells, measured at 60 °C from 1.0 to 5.0 V vs Li^+/Li, with a scan rate of 100 $\mu V\ s^{-1}$. An enlarged view is shown in (b). The electrochemical stability was assessed on the basis of the decomposition occurring at the first edge potential (E_{onset}), i.e., the potential where a faradic current is detectable.[30]

PARSTAT MC/PMC-1000 at C/20 (12 mA/g), C/10, C/5, C/2, and C.

3. RESULTS AND DISCUSSION

Figure 1a shows the X-ray diffraction pattern of the *h*-$Li(BH_4)_{0.8}(I)_{0.2}$-SiO_2 (solid-state electrolyte, i.e., SSE), in which the only crystalline phase observed is *h*-$Li(BH_4)_{0.8}(I)_{0.2}$ (see Figure S1 for comparison with the pattern of the *h*-$Li(BH_4)_{0.8}(I)_{0.2}$). The crystalline structure of the SSE in Rietveld refinement (Figure 1a) was defined using the starting structure of the hexagonal polymorph of *h*-$LiBH_4$ (*P*63*mc*),[24] in which, however, I^- ions occupy 20% of the boron positions (i.e., 2b Wyckoff site, $x = 0.3333$, $y = 0.6667$, $z = 0.553$). The structure resulting from the Rietveld refinement is shown in the inset in Figure 1a, where a small increase of the I^- z coordinate, i.e., $x = 0.3333$, $y = 0.6667$, and $z = 0.602$, and a larger cell volume (57.1 $Å^3$) than the RT extrapolated volume of *h*-$LiBH_4$ (53.3 $Å^3$), see Table S2) was detected. Expansion of the lattice is expected as the radius of I^- is larger than that of BH_4^- (I^- = 2.20 Å, BH_4^- = 2.03 Å).[25]

The SSE was further analyzed with infrared spectroscopy in Attenuated Total Reflection mode (Figure 1b). The *h*-$Li(BH_4)_{0.8}(I)_{0.2}$ spectrum shows new bands, compared to the *o*-$LiBH_4$ spectra, at ~1170 cm^{-1} and 960 cm^{-1}, in agreement with results reported by Rude et al.[26]. The absorption bands related to B−H stretching (2400−2000 cm^{-1} region) of the *h*-$Li(BH_4)_{0.8}(I)_{0.2}$ and SSE are similar, but they differ from that of *o*-$LiBH_4$, which reflects a different symmetry of the BH_4^- anions due to the stabilization of the hexagonal phase.[26,27] Furthermore, the presence of the SiO_2 is evident from the intense and broad absorption band in the SSE spectrum in the region 1300−750 cm^{-1}. Finally, the N_2 absorption performed on the SSE sample showed a surface area (25 m^2/g_{SSE}) and pore volume (0.1 cm^3/g_{SSE}), which decreased by an order of magnitude compared to the SiO_2 (i.e., 294 m^2/g, 2.30 cm^3/g, respectively, see Figure S2 and Table S3), confirming that the mechanochemical treatment allows to form a dense nanocomposite.

Figure 1c shows the conductivity versus inverse temperature of the SSE, including, for a comparison, results obtained for pure $LiBH_4$. Figure 1d shows the conductivity comparison between *h*-$Li(BH_4)_{0.8}(I)_{0.2}$ with and without SiO_2 added. With SiO_2, the conductivity at 40 °C is 9.3×10^{-5} S cm^{-1}, similar to the value reported for $LiBH_4$-LiI-SBA-15 prepared by nanoconfinement (1.3×10^{-4} S cm^{-1}).[21] The RT conductivity is about 4 orders of magnitude higher than for pure $LiBH_4$, and it is slightly higher than that of the *h*-$Li(BH_4)_{0.8}(I)_{0.2}$ at the same temperature (see Figure 1d). The activation energy (E_A) for SSE sample, obtained from a linear fit ($R^2 > 0.999$) of the $\ln(\sigma T)$ versus $1/T$ data shown in Figure 1d, was 0.51 ± 0.01 eV. The E_A obtained for SSE is similar to that of the pure *h*-$Li(BH_4)_{0.8}(I)_{0.2}$ (i.e., 0.55 ± 0.02 eV), but much lower than the E_A of *o*-$LiBH_4$ (i.e., 0.75 ± 0.07 eV).[28] A sudden change in the conductivity above 110 °C due to the polymorphic transition was observed for pure $LiBH_4$ but, as expected, not for the hexagonal solid solution.

Similar to $LiBH_4$-oxide composites,[15] the enhancement of the conductivity due to the silica incorporation can be explained using a core−shell model (see Figure S3 for a graphical view), in which two different fractions are present: (a) the region between the *h*-$Li(BH_4)_{0.8}(I)_{0.2}$ and the oxide, which forms a highly conductive layer; (b) the bulk region, maintaining the conductivity of the hexagonal *h*-Li-

https://doi.org/10.1021/acs.jpcc.2c08902
J. Phys. Chem. C 2023, 127, 3988−3995

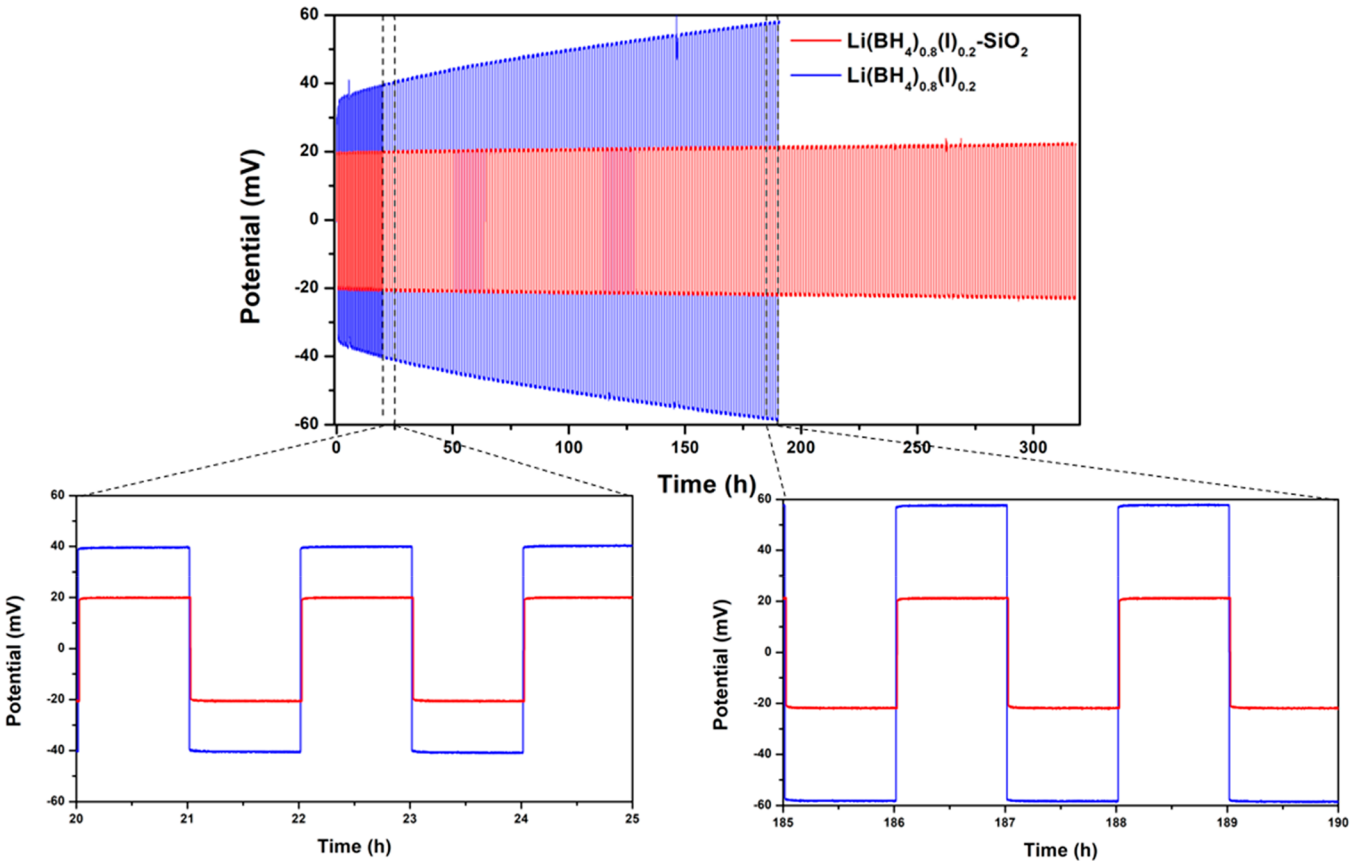

Figure 3. Cycling profiles of the symmetrical Li|*h*-$Li(BH_4)_{0.8}(I)_{0.2}$|Li (blue) and Li|SSE|Li (red) cells at 60 °C with a constant current density of 0.031 mA/cm^2 applied for 30 min, in the initial 20 cycles, and for 1 h for the following cycles..

$(BH_4)_{0.8}(I)_{0.2}$ phase.[14,15,18] Taking into consideration an interfacial SSE-SiO_2 layer thickness of 2 nm,[15,20] the calculation of the theoretical thickness (Table S1), based on our previous studies,[15,19] confirms that there is some bulk *h*-$Li(BH_4)_{0.8}(I)_{0.2}$ that is far from the interface layer, yet able to form a well-connected pathway for the Li-ion conduction. This is based on the assumption that the interface layer thickness of the $LiBH_4$−SiO_2 and *h*-$Li(BH_4)_{0.8}(I)_{0.2}$-SiO_2 are equal, because the calorimetric procedure to probe the phase transition temperature, as used by Suwarno et al.,[20] cannot be used in this case, as the transition has already been suppressed by the I^- substitution. These results demonstrate that the combination of the two different approaches to increase the Li-ion conductivity is a powerful synthesis route for solid-state electrolytes with ionic conductivities suitable for application in all-solid-state batteries.[21,29]

To establish whether the mechanical treatment with silica has an influence on the electrochemical stability window, cyclic voltammetry was performed on both the SSE and *h*-$Li(BH_4)_{0.8}(I)_{0.2}$ at 60 °C (Figure 2).

A small anodic peak (E_{onset}), at about 2.5 and 2.6 V, was detected for the *h*-$Li(BH_4)_{0.8}(I)_{0.2}$ and SSE, respectively, assigned to the partial decomposition of the of BH_4^-.[11,23] At higher potentials (above 3.0 V), a major oxidative event is observed for both samples, that is assigned to the extraction of the I^- ion from the crystal structure above 3.0 V.[31,32]

The oxidation stability of a mixture, is determined by the stability of the least stable anion, which sets the practical stability limit of the whole binary compound.[33] The electrochemical stability window of the SSE can therefore be defined as about 2.5 V, determined by the decomposition potential of the BH_4^-. The electrochemical stability window of pure $LiBH_4$ is around 2.2 V versus Li^+/Li,[11,23] and similar results was obtained for $LiBH_4$−MgO nanocomposites (2.2 V vs Li^+/Li).[19] These findings confirm that the mechanical treatment enhances the ionic conductivity without altering the oxidative stability of the electrolyte.

The compatibility of *h*-$Li(BH_4)_{0.8}(I)_{0.2}$ and SSE with Li metal anodes was explored by assembling symmetric Li metal cells. Figure 3 depicts the evolution of the cell voltage profile over time, at a constant current of 0.031 mA/cm^2 at intervals of 30 min (for the first 20 steps, 6 μAh/cm^2) and 1 h (for following steps, 0.031 mAh/cm^2). The cell containing only the *h*-$Li(BH_4)_{0.8}(I)_{0.2}$ without silica nanoparticles, showed an increasing polarization upon cycling. The overpotential reached 58 mV (47% higher than the initial value of 40 mV, i.e., from an initial total resistance of 1643 Ω to a final of 2383 Ω) before the cell shorted after 185 h (7.5 days), suggesting a limited stability against lithium metal. The higher initial voltage, compared to the results obtained for the SSE, can be due to (a) slightly lower ionic conductivity; (b) occurrence of parasitic reactions; (c) poor interfacial contact. Differently, the earlier short circuit (after 185 and 300 h for *h*-$Li(BH_4)_{0.8}(I)_{0.2}$ and SSE, respectively) might be due to a lower mechanical strength compared to the SSE, i.e., limited ability to stop dendritic growth. In contrast, for the cell containing the SSE, lithium plating and stripping is fully reversibly, with a low potential, that reaches 21 mV as maximum value (5% higher than the initial polarization of 20 mV). Importantly, the overall voltage remains constant for almost 300 h (12.5 days),

https://doi.org/10.1021/acs.jpcc.2c08902
J. Phys. Chem. C 2023, 127, 3988−3995

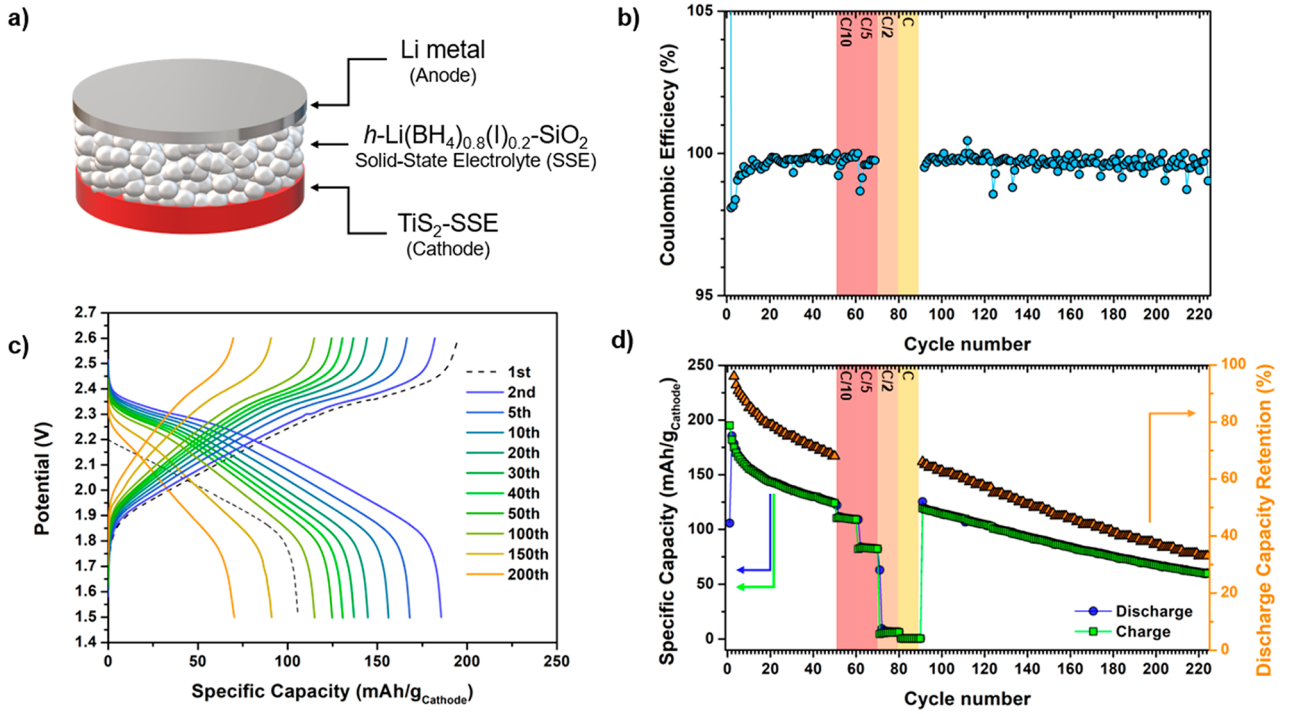

Figure 4. (a) Schematic illustration of the assembled all-solid-state battery (SSB). (b) Coulombic efficiency (charge capacity over discharge capacity). (c) Voltage profiles of Li|SSE|TiS_2 solid-state battery during cycling at 60 °C, selected voltage profiles are presented. (d) Discharge/charge specific capacity (left) and discharge capacity retention ratio (right) as a function of the cycle number for a rate of C/20 (12 mA/g), C/10, C/5, C/2, and C. The capacity of the battery is expressed in mAh per g of TiS_2.

indicating that the electrolyte is stable in contact with lithium. The value of 21 mV is in line with the EIS spectra (Figure S4) collected on the as-assembled cell, resulting in a contact/interface resistance, after having subtracted the electrolyte contribution, equal to 165 Ω cm^2, that can be caused by the absence of a controlled cell stack pressure.[2,34,35] These results suggest that the addition of silica nanoparticles increase the stability of the electrolyte for lithium stripping and plating.

The different behaviors shown by the symmetric cells (Figure 3) could tentatively be explained by an improved mechanical strength of the SSE, compared to the *h*-$Li(BH_4)_{0.8}(I)_{0.2}$, induced by the addition of SiO_2.[2] The theoretical bulk modulus of $LiBH_4$ is 10−20 GPa.[36] Such a low bulk modulus compared to other solid-state electrolytes[37] is advantageous for mechanical processing.[38] At the same time, to prevent Li dendrite growth, the shear modulus should be at least twice that of the lithium metal,[39,40] but that of $LiBH_4$ is only slightly larger than that of Li (i.e., 5.12 GPa for $LiBH_4$ vs 4.02 GPa for Li metal).[36] The addition of harder materials, e.g., SiO_2 with an shear modulus of 30−40 GPa,[41,42] could increase the SSE rigidity preventing the formation of Li dendrites.

Similar behavior has been observed for polymer-based solid electrolytes, in which the mechanical properties were improved by the presence of oxide particles.[43,44] Recently, it was demonstrated that addition of Si nanoparticles can inhibit the formation of Li dendrites at the interface of Li anode.[45] However, a detailed study of the mechanical strength and the effect of pressure is outside the scope of the present work.

Given its high ionic conductivity and excellent stability in plating/stripping lithium, an all-solid-state Li/TiS_2 battery was assembled (Figure 4a). Figure 4c shows the charge−discharge voltage profiles for cycling at 60 °C between 1.5 and 2.6 V at C/20. C-rate-capability tests (C/10, C/5, C/2, C, 10 cycles each) were performed. The SSB exhibits a reversible charge capacity of 181 mAh/g and discharge capacity of 185 mAh/g in the second cycle, that corresponds to about 76 and 77%, respectively, of the theoretical capacity of TiS_2 (239 mAh/g).[46−48] Optimization of the cathode mixture and preparation could enable higher initial capacity.[49] The battery was successfully cycled for more than 220 times, i.e., to our knowledge, the longest cyclability reached by an SSB using a $LiBH_4$-based electrolyte, showing a discharge capacity retention of 68% after 50 cycles, and 34% after 220 cycles (Figure 4d). Moreover, the Coulombic efficiency remained between 99% and 100% during the first 70 cycles, i.e., also at the C-rate of C/10 and C/5, as well as from the 90th to 220th cycle (Figure 4b). During the C-rate capability test, while the Coulombic efficiency remained stable, the capacity slightly decreased with increasing C-rate, until C/5. Nevertheless, this is the highest C-rate achieved by an SSB assembled using a $LiBH_4$-based SSE (see Table S4 for the comparison). Subsequent increase in C-rate (from C/2 to C) deeply affect the cell performances, with a drastic reduction of the specific capacity, likely due to an insufficient Li-ion conductivity of the SSE.

A significant difference was observed between the discharge capacity of the first and the second cycle (106 and 185 mAh/g). This is related to reactions at the TiS_2/$LiBH_4$-based-electrolyte interface to possibly form $Li_2B_{12}H_{12}$ and other compounds.[50] Such decomposition is likely kinetically limited above a critical thickness of $Li_2B_{12}H_{12}$, resulting in a stable solid electrode interface layer.[19,50] Similar behavior has been reported for Li-TiS_2 SSBs by Unemoto et al.[50] for a $LiBH_4$ electrolyte at 120 °C, for a $LiBH_4$-MgO electrolyte at 60 °C[19] and also in Li-S SSB based on $LiBH_4$-SiO_2 electrolytes.[51]

https://doi.org/10.1021/acs.jpcc.2c08902
J. Phys. Chem. C 2023, 127, 3988−3995

The cell impedance was monitored after each charge/discharge cycle (Figure S5). Figure S5a shows the Nyquist plot after the cell was assembled (before charge/discharge cycles) and after every 10 charge−discharge cycles. Figure S5b shows that the contact resistance of the fresh cell is <1 Ω (similar to that obtained by Kim et al.[52]). After this initial low resistance value, the contact resistance increases, explaining also the capacity fading. The capacity fading can be caused by two contributions: (a) the formation of the $Li_2B_{12}H_{12}$-based SEI layer and (b) the loss of contact at the electrodes interfaces.[19]

The satisfactory cycling performance of the cell suggests that the studied SSE can be adopted as a solid electrolyte for SSB. A key point that should not be overlooked is that a much higher charge/discharge cycles have been performed by the cell assembled in this work, compared to those where $LiBH_4$-base electrolytes and Li metal as anode were used (see table in ref 53), proving that the addition of SiO_2 nanoparticles improves also the cycling properties. While we have obtained exceptional cycling behavior in the studied system, the battery performance could (likely) be further improved by optimizing the contact between the electrolyte and the electrodes, as well as employing other cathodes materials.

4. CONCLUSIONS

In this work, the effect of nanocomposite formation via ball milling on the electrochemical properties of halogenated $LiBH_4$ (h-$Li(BH_4)_{0.8}(I)_{0.2}$) has been investigated. The h-$Li(BH_4)_{0.8}(I)_{0.2}$-SiO_2 demonstrated a higher conductivity than pristine $LiBH_4$ and the pure solid solution. The electrochemical stability window of the nanocomposite is similar to that of the solid solution but the stability against Li-metal is drastically improved by the presence of the oxide nanoparticles. We ascribed this to the fact that the addition of the rigid SiO_2 nanoparticles which has a high shear modulus, strengthens the SSE, likely mitigating the dendrite propagation. Importantly, we have assembled an all-solid state battery cell (Li|h-$Li(BH_4)_{0.8}(I)_{0.2}$-SiO_2|TiS_2) that shows a long-term cyclability, i.e., over 200 cycles, demonstrating that the addition of oxide nanoparticles significantly improves the stability of the solid electrolytes. We believe that further optimization of the cathode composition and preparation could improve the battery performance, opening potential for applications for instance in stationary storage.

■ ASSOCIATED CONTENT

Supporting Information

The Supporting Information is available free of charge at https://pubs.acs.org/doi/10.1021/acs.jpcc.2c08902.

Description of the synthesis and composition details. N_2 physisorption isotherms, Li-ion conductivity, XRD pattern, and Rietveld refinement parameters of the h-$Li(BH_4)_{0.8}(I)_{0.2}$ and h-$Li(BH_4)_{0.8}(I)_{0.2}$-SiO_2. Nyquist plot of the fresh assembled symmetric cell and battery cell and as a function of the battery cycles (PDF)

■ AUTHOR INFORMATION

Corresponding Authors

Valerio Gulino − *Materials Chemistry and Catalysis, Debye Institute for Nanomaterials Science, Utrecht University, 3584 CG Utrecht, The Netherlands; Department of Chemistry and NIS - INSTM, University of Turin, 10125 Torino, Italy;* orcid.org/0000-0002-5808-7802; Phone: +39 3804624454; Email: v.gulino@uu.nl

Petra de Jongh − *Materials Chemistry and Catalysis, Debye Institute for Nanomaterials Science, Utrecht University, 3584 CG Utrecht, The Netherlands*; Phone: +31 30 2531747; Email: p.r.dejongh@uu.nl

Authors

Laura de Kort − *Materials Chemistry and Catalysis, Debye Institute for Nanomaterials Science, Utrecht University, 3584 CG Utrecht, The Netherlands*

Peter Ngene − *Materials Chemistry and Catalysis, Debye Institute for Nanomaterials Science, Utrecht University, 3584 CG Utrecht, The Netherlands;* orcid.org/0000-0003-3691-0623

Marcello Baricco − *Department of Chemistry and NIS - INSTM, University of Turin, 10125 Torino, Italy;* orcid.org/0000-0002-2856-9894

Complete contact information is available at: https://pubs.acs.org/10.1021/acs.jpcc.2c08902

Author Contributions

V.G. and P.d.J. designed the research. V.G. carried out the syntheses, measurements, data analyses, and wrote the manuscript. L.K. assisted in the electrochemical measurements and helped in the writing process. P.N., M.B., and P.d.J. participated in discussions of the results, supervised the research, and commented on the manuscript.

Notes

The authors declare no competing financial interest.

■ ACKNOWLEDGMENTS

Financial support from The Netherlands Organization for Scientific Research (NWO-ECHO and NOW-RELEASE) is gratefully acknowledged. The authors kindly acknowledge Jan Willem de Rijk and Marcel Van Asselen for technical support in the laboratory

■ REFERENCES

(1) Goodenough, J. B.; Kim, Y. Challenges for Rechargeable Li Batteries †. *Chem. Mater.* **2010**, *22* (3), 587−603.

(2) Brighi, M.; Murgia, F.; Černý, R. Mechanical Behavior and Dendrite Resistance of Closo-Hydroborate Solid Electrolyte. *Adv. Mater. Interfaces* **2022**, *9* (3), 2101254.

(3) de Kort, L. M.; Gulino, V.; de Jongh, P. E.; Ngene, P. Ionic Conductivity in Complex Metal Hydride-Based Nanocomposite Materials: The Impact of Nanostructuring and Nanocomposite Formation. *J. Alloys Compd.* **2022**, *901*, 163474.

(4) Cuevas, F.; Amdisen, M. B.; Baricco, M.; Buckley, C. E.; Cho, Y. W.; de Jongh, P.; de Kort, L. M.; Grinderslev, J. B.; Gulino, V.; Hauback, B. C.; et al. Metallic and Complex Hydride-Based Electrochemical Storage of Energy. *Prog. Energy* **2022**, *4* (3), 032001.

(5) Dematteis, E. M.; Amdisen, M. B.; Autrey, T.; Barale, J.; Bowden, M. E.; Buckley, C. E.; Cho, Y. W.; Deledda, S.; Dornheim, M.; de Jongh, P.; et al. Hydrogen Storage in Complex Hydrides: Past Activities and New Trends. *Prog. Energy* **2022**, *4* (3), 032009.

(6) El Kharbachi, A.; Pinatel, E.; Nuta, I.; Baricco, M. A Thermodynamic Assessment of $LiBH_4$. *Calphad* **2012**, *39*, 80−90.

(7) Matsuo, M.; Nakamori, Y.; Orimo, S.; Maekawa, H.; Takamura, H. Lithium Superionic Conduction in Lithium Borohydride Accompanied by Structural Transition. *Appl. Phys. Lett.* **2007**, *91* (22), 224103.

(8) Sveinbjörnsson, D.; Myrdal, J. S. G.; Blanchard, D.; Bentzen, J. J.; Hirata, T.; Mogensen, M. B.; Norby, P.; Orimo, S.; Vegge, T. Effect of

Heat Treatment on the Lithium Ion Conduction of the $LiBH_4$-LiI Solid Solution. *J. Phys. Chem. C* **2013**, *117* (7), 3249−3257.
(9) Maekawa, H.; Matsuo, M.; Takamura, H.; Ando, M.; Noda, Y.; Karahashi, T.; Orimo, S.-i. Halide-Stabilized $LiBH_4$, a Room-Temperature Lithium Fast-Ion Conductor. *J. Am. Chem. Soc.* **2009**, *131* (3), 894−895.
(10) Gulino, V.; Dematteis, E. M.; Corno, M.; Palumbo, M.; Baricco, M. Theoretical and Experimental Studies of $LiBH_4$-LiBr Phase Diagram. *ACS Appl. Energy Mater.* **2021**, *4* (7), 7327−7337.
(11) Gulino, V.; Brighi, M.; Dematteis, E. M.; Murgia, F.; Nervi, C.; Černý, R.; Baricco, M. Phase Stability and Fast Ion Conductivity in the Hexagonal $LiBH_4$-LiBr-LiCl Solid Solution. *Chem. Mater.* **2019**, *31* (14), 5133−5144.
(12) Zhu, M.; Pang, Y.; Lu, F.; Shi, X.; Yang, J.; Zheng, S. In Situ Formed Li-B-H Complex with High Li-Ion Conductivity as a Potential Solid Electrolyte for Li Batteries. *ACS Appl. Mater. Interfaces* **2019**, *11* (15), 14136−14141.
(13) de Kort, L. M.; Gulino, V.; Blanchard, D.; Ngene, P. Effects of $LiBF_4$ Addition on the Lithium-Ion Conductivity of $LiBH_4$. *Molecules* **2022**, *27* (7), 2187.
(14) Blanchard, D.; Nale, A.; Sveinbjörnsson, D.; Eggenhuisen, T. M.; Verkuijlen, M. H. W.; Suwarno; Vegge, T.; Kentgens, A. P. M.; de Jongh, P. E. Nanoconfined $LiBH_4$ as a Fast Lithium Ion Conductor. *Adv. Funct. Mater.* **2015**, *25* (2), 184−192.
(15) Gulino, V.; Barberis, L.; Ngene, P.; Baricco, M.; de Jongh, P. E. Enhancing Li-Ion Conductivity in $LiBH_4$-Based Solid Electrolytes by Adding Various Nanosized Oxides. *ACS Appl. Energy Mater.* **2020**, *3* (5), 4941−4948.
(16) Lambregts, S. F. H.; van Eck, E. R. H.; Suwarno; Ngene, P.; de Jongh, P. E.; Kentgens, A. P. M. Phase Behavior and Ion Dynamics of Nanoconfined $LiBH_4$ in Silica. *J. Phys. Chem. C* **2019**, *123* (42), 25559−25569.
(17) Zettl, R.; Hogrefe, K.; Gadermaier, B.; Hanzu, I.; Ngene, P.; de Jongh, P. E.; Wilkening, H. M. R. Conductor-Insulator Interfaces in Solid Electrolytes: A Design Strategy to Enhance Li-Ion Dynamics in Nanoconfined $LiBH_4/Al_2O_3$. *J. Phys. Chem. C* **2021**, *125* (27), 15052−15060.
(18) Zettl, R.; Gombotz, M.; Clarkson, D.; Greenbaum, S. G.; Ngene, P.; de Jongh, P. E.; Wilkening, H. M. R. Li-Ion Diffusion in Nanoconfined $LiBH_4$-LiI/Al_2O_3: From 2D Bulk Transport to 3D Long-Range Interfacial Dynamics. *ACS Appl. Mater. Interfaces* **2020**, *12* (34), 38570−38583.
(19) Gulino, V.; Brighi, M.; Murgia, F.; Ngene, P.; de Jongh, P.; Černý, R.; Baricco, M. Room-Temperature Solid-State Lithium-Ion Battery Using a $LiBH_4$-MgO Composite Electrolyte. *ACS Appl. Energy Mater.* **2021**, *4* (2), 1228−1236.
(20) Suwarno; Ngene, P.; Nale, A.; Eggenhuisen, T. M.; Oschatz, M.; Embs, J. P.; Remhof, A.; De Jongh, P. E. Confinement Effects for Lithium Borohydride: Comparing Silica and Carbon Scaffolds. *J. Phys. Chem. C* **2017**, *121* (8), 4197−4205.
(21) Zettl, R.; de Kort, L.; Gombotz, M.; Wilkening, H. M. R.; de Jongh, P. E.; Ngene, P. Combined Effects of Anion Substitution and Nanoconfinement on the Ionic Conductivity of Li-Based Complex Hydrides. *J. Phys. Chem. C* **2020**, *124* (5), 2806−2816.
(22) Lu, F.; Pang, Y.; Zhu, M.; Han, F.; Yang, J.; Fang, F.; Sun, D.; Zheng, S.; Wang, C. A High-Performance Li-B-H Electrolyte for All-Solid-State Li Batteries. *Adv. Funct. Mater.* **2019**, *29* (15), 1809219.
(23) Asakura, R.; Duchêne, L.; Kühnel, R.-S.; Remhof, A.; Hagemann, H.; Battaglia, C. Electrochemical Oxidative Stability of Hydroborate-Based Solid-State Electrolytes. *ACS Appl. Energy Mater.* **2019**, *2* (9), 6924−6930.
(24) Soulie, J.; Renaudin, G.; Černý, R.; Yvon, K. Lithium Boro-Hydride $LiBH_4$ I. Crystal Structure. *J. Alloys Compd.* **2002**, *346*, 200−205.
(25) Paskevicius, M.; Jepsen, L. H.; Schouwink, P.; Černý, R.; Ravnsbæk, D. B.; Filinchuk, Y.; Dornheim, M.; Besenbacher, F.; Jensen, T. R. Metal Borohydrides and Derivatives - Synthesis, Structure and Properties. *Chem. Soc. Rev.* **2017**, *46* (5), 1565−1634.
(26) Rude, L. H.; Zavorotynska, O.; Arnbjerg, L. M.; Ravnsbæk, D. B.; Malmkjær, R. A.; Grove, H.; Hauback, B. C.; Baricco, M.; Filinchuk, Y.; Besenbacher, F.; Jensen, T. R. Bromide Substitution in Lithium Borohydride, $LiBH_4$-LiBr. *Int. J. Hydrogen Energy* **2011**, *36* (24), 15664−15672.
(27) Rude, L. H.; Groppo, E.; Arnbjerg, L. M.; Ravnsbæk, D. B.; Malmkjær, R. A.; Filinchuk, Y.; Baricco, M.; Besenbacher, F.; Jensen, T. R. Iodide Substitution in Lithium Borohydride, $LiBH_4$-LiI. *J. Alloys Compd.* **2011**, *509* (33), 8299−8305.
(28) Gulino, V.; Wolczyk, A.; Golov, A. A.; Eremin, R. A.; Palumbo, M.; Nervi, C.; Blatov, V. A.; Proserpio, D. M.; Baricco, M. Combined DFT and Geometrical-Topological Analysis of Li-Ion Conductivity in Complex Hydrides. *Inorg. Chem. Front.* **2020**, *7* (17), 3115−3125.
(29) de Kort, L. M.; Harmel, J.; de Jongh, P. E.; Ngene, P. The Effect of Nanoscaffold Porosity and Surface Chemistry on the Li-Ion Conductivity of $LiBH_4$-$LiNH_2$/Metal Oxide Nanocomposites. *J. Mater. Chem. A* **2020**, *8* (39), 20687−20697.
(30) Espinoza, E. M.; Clark, J. A.; Soliman, J.; Derr, J. B.; Morales, M.; Vullev, V. I. Practical Aspects of Cyclic Voltammetry: How to Estimate Reduction Potentials When Irreversibility Prevails. *J. Electrochem. Soc.* **2019**, *166* (5), H3175−H3187.
(31) Armstrong, R. D.; Landles, K. Electrochemical Behaviour of Lithium Iodide Monohydrate. *J. Appl. Electrochem.* **1981**, *11* (2), 247−251.
(32) Sveinbjörnsson, D.; Christiansen, A. S.; Viskinde, R.; Norby, P.; Vegge, T. The $LiBH_4$-LiI Solid Solution as an Electrolyte in an All-Solid-State Battery. *J. Electrochem. Soc.* **2014**, *161* (9), A1432−A1439.
(33) Brighi, M.; Murgia, F.; Černý, R. Closo-Hydroborate Sodium Salts as an Emerging Class of Room-Temperature Solid Electrolytes. *Cell Reports Phys. Sci.* **2020**, *1*, 100217.
(34) Sakamoto, J. More Pressure Needed. *Nat. Energy* **2019**, *4* (10), 827−828.
(35) Wang, M. J.; Choudhury, R.; Sakamoto, J. Characterizing the Li-Solid-Electrolyte Interface Dynamics as a Function of Stack Pressure and Current Density. *Joule* **2019**, *3* (9), 2165−2178.
(36) Lu, Z.; Ciucci, F. Metal Borohydrides as Electrolytes for Solid-State Li, Na, Mg, and Ca Batteries: A First-Principles Study. *Chem. Mater.* **2017**, *29* (21), 9308−9319.
(37) Deng, Z.; Wang, Z.; Chu, I.-H.; Luo, J.; Ong, S. P. Elastic Properties of Alkali Superionic Conductor Electrolytes from First Principles Calculations. *J. Electrochem. Soc.* **2016**, *163* (2), A67−A74.
(38) Duchêne, L.; Remhof, A.; Hagemann, H.; Battaglia, C. Status and Prospects of Hydroborate Electrolytes for All-Solid-State Batteries. *Energy Storage Mater.* **2020**, *25* (May), 782.
(39) Monroe, C.; Newman, J. The Impact of Elastic Deformation on Deposition Kinetics at Lithium/Polymer Interfaces. *J. Electrochem. Soc.* **2005**, *152* (2), A396.
(40) Yu, S.; Schmidt, R. D.; Garcia-Mendez, R.; Herbert, E.; Dudney, N. J.; Wolfenstine, J. B.; Sakamoto, J.; Siegel, D. J. Elastic Properties of the Solid Electrolyte $Li_7La_3Zr_2O_{12}$ (LLZO). *Chem. Mater.* **2016**, *28* (1), 197−206.
(41) Pabst, W.; Gregorová, E. Elastic Properties of Silica Polymorphs-a Review. *Ceram. - Silikaty* **2013**, *57* (3), 167−184.
(42) An, L.; Zhang, D.; Zhang, L.; Feng, G. Effect of Nanoparticle Size on the Mechanical Properties of Nanoparticle Assemblies. *Nanoscale* **2019**, *11* (19), 9563−9573.
(43) Xue, Z.; He, D.; Xie, X. Poly(Ethylene Oxide)-Based Electrolytes for Lithium-Ion Batteries. *J. Mater. Chem. A* **2015**, *3* (38), 19218−19253.
(44) Shang, S. W.; Williams, J. W.; Söderholm, K.-J. M. Work of Adhesion Influence on the Rheological Properties of Silica Filled Polymer Composites. *J. Mater. Sci.* **1995**, *30* (17), 4323−4334.
(45) Tao, J.; Wang, D.; Yang, Y.; Li, J.; Huang, Z.; Mathur, S.; Hong, Z.; Lin, Y. Swallowing Lithium Dendrites in All-Solid-State Battery by Lithiation with Silicon Nanoparticles. *Adv. Sci.* **2022**, *9* (4), 2103786.
(46) Dahn, J.; Haering, R. R. Lithium Intercalation in TiS2. *Mater. Res. Bull.* **1979**, *14* (10), 1259−1262.

https://doi.org/10.1021/acs.jpcc.2c08902
J. Phys. Chem. C 2023, 127, 3988−3995

(47) Dahn, J. R.; McKinnon, W. R.; Haering, R. R.; Buyers, W. J. L.; Powell, B. M. Structure Determination of Li x TiS 2 by Neutron Diffraction. *Can. J. Phys.* **1980**, *58* (2), 207−213.
(48) Dahn, J. R.; Haering, R. R. Anomalous Bragg Peak Widths in Li_xTiS_2. *Solid State Commun.* **1981**, *40* (3), 245−248.
(49) Duchêne, L.; Kim, D. H.; Song, Y. B.; Jun, S.; Moury, R.; Remhof, A.; Hagemann, H.; Jung, Y. S.; Battaglia, C. Crystallization of Closo-Borate Electrolytes from Solution Enabling Infiltration into Slurry-Casted Porous Electrodes for All-Solid-State Batteries. *Energy Storage Mater.* **2020**, *26*, 543−549.
(50) Unemoto, A.; Ikeshoji, T.; Yasaku, S.; Matsuo, M.; Stavila, V.; Udovic, T. J.; Orimo, S. I. Stable Interface Formation between TiS_2 and $LiBH_4$ in Bulk-Type All-Solid-State Lithium Batteries. *Chem. Mater.* **2015**, *27* (15), 5407−5416.
(51) Das, S.; Ngene, P.; Norby, P.; Vegge, T.; de Jongh, P. E.; Blanchard, D. All-Solid-State Lithium-Sulfur Battery Based on a Nanoconfined $LiBH_4$ Electrolyte. *J. Electrochem. Soc.* **2016**, *163* (9), A2029−A2034.
(52) Kim, S.; Oguchi, H.; Toyama, N.; Sato, T.; Takagi, S.; Otomo, T.; Arunkumar, D.; Kuwata, N.; Kawamura, J.; Orimo, S. A Complex Hydride Lithium Superionic Conductor for High-Energy-Density All-Solid-State Lithium Metal Batteries. *Nat. Commun.* **2019**, *10* (1), 1081.
(53) Latroche, M.; Blanchard, D.; Cuevas, F.; El Kharbachi, A.; Hauback, B. C.; Jensen, T. R.; de Jongh, P. E.; Kim, S.; Nazer, N. S.; Ngene, P.; et al. Full-Cell Hydride-Based Solid-State Li Batteries for Energy Storage. *Int. J. Hydrogen Energy* **2019**, *44* (15), 7875−7887.

Recommended by ACS

***In Situ* Construction of S-Based Artificial Solid Electrolyte Interphases Layer for Stable Silicon Anode in Lithium-Ion Batteries**

Weilun Chen, Yunhui Huang, *et al.*
NOVEMBER 02, 2022
ACS APPLIED ENERGY MATERIALS
READ

Prefabrication of "Trinity" Functional Binary Layers on a Silicon Surface to Develop High-Performance Lithium-Ion Batteries

Weibo Huang, Honghe Zheng, *et al.*
JANUARY 25, 2023
ACS NANO
READ

Monolithic 100% Silicon Wafer Anode for All-Solid-State Batteries Achieving High Areal Capacity at Room Temperature

Ikcheon Na, Jongwoo Lim, *et al.*
MARCH 27, 2023
ACS ENERGY LETTERS
READ

Electrochemical Synthesis of Binary Structured Clusters Based on Si Nanoparticles and Si Nanowires for High-Performance Lithium-Ion Battery Anodes

Qiang Yu, Xiaocheng Li, *et al.*
NOVEMBER 08, 2022
ACS APPLIED NANO MATERIALS
READ

https://doi.org/10.1021/acs.jpcc.2c08902
J. Phys. Chem. C 2023, 127, 3988−3995